Available online at www.eccomasproceedia.org
Eccomas Proceedia COMPDYN (2023) 1731-1743

ECCOMAS
Proceedia

COMPDYN 2023
9th ECCOMAS Thematic Conference on
Computational Methods in Structural Dynamics and Earthquake Engineering
M. Papadrakakis, M. Fragiadakis (eds.)
Athens, Greece, 12-14 June 2023

EFFECTS OF AGING AND DETERIORATION ON THE SEISMIC FRAGILITY OF MASONRY ARCH BRIDGES

Giovanni Tecchio[1], Sara Barbisan[2], Elisa Saler[1], Francesca da Porto[1]

[1] Department of Geosciences, University of Padova
Via Gradenigo 6, 35131 Padova, Italy
{giovanni.tecchio; elisa.saler; francesca.daporto}@unipd.it

[2] Department of Civil, Architectural and Environmental Engineering, University of Padova
Via Marzolo 9, 35131 Padova, Italy
sara.barbisan@dicea.unipd.it

Abstract

This contribution presents the derivation of numerical seismic fragility sets for masonry arch bridges including the effects of typical defects, i.e., material loss at the intrados of the arch, material degradation, and longitudinal cracks of the arch barrel vault. Fragility curves were derived for single-span structures providing fragility sets for two bridge macro-classes, i.e., semi-circular and segmental. The evaluation was carried out through 2D finite-element modelling, by implementing parametric nonlinear static analyses on 32 reference bridges for each macro-class. For modelling material loss at the intrados, a number of elements of the numerical mesh were removed; for material degradation the masonry properties were reduced; lastly, longitudinal cracks were implemented by simulating the reduction of the barrel's effective width, as this defect often cause the detachment of spandrels from the arch barrel. For each deterioration effect, two level of severity were assumed. The variability related to the seismic demand was included by deriving sets of elastic spectra from ground motion records selected according to multiple-stripe analysis, with peak ground accelerations ranging from 0.05 to 1.5 g. Derived fragility sets showed an appreciable increase in seismic vulnerability of masonry bridges when the effects of degradation are included in the evaluation, with a greater influence given by material loss.

Keywords: masonry arch bridges, fragility curves, ageing effects, damage effects, nonlinear static analyses, finite-element modelling

ISSN:2623-3347
Peer-review under responsibility of the organizing committee of COMPDYN 2023.
doi: 10.7712/120123.10515.20969

1 INTRODUCTION

Masonry arch bridges represent 40% of existing bridges in European transportation railway network, being of crucial importance in transport systems. Given their widespread, masonry arch bridges are commonly found in seismic areas, such as Italy. Moreover, these bridges are strongly aged; for example, according to the inventory of the Italian State Railways, they were mainly built between 1840 and 1930. Seismic risk assessment of transport networks, which are crucial in post-event emergency, should therefore include masonry bridges. In the Italian context, the inventory of railways masonry bridges (IrMB) counts more than 56,000 structures, which are mainly single-span bridges, built between 1840 and 1930 [1,2].

Fragility models of this macro-class of bridges are therefore required to carry out seismic risk analyses of railway networks at a territorial scale. However, despite their frequency, especially in railway networks, masonry arch bridges were less investigated than other types, such as reinforced concrete (r.c.) bridges. Most of these studies focused on the 'as-built' configuration of these structures, neglecting deterioration and damage effects [3,4].

Nevertheless, realistic risk assessment of bridges requires considering the state of deterioration, which was demonstrated to affect their capacity and dynamic response [5,6]. Most previous studies investigated the effects of deterioration on seismic fragility for r.c. structures [7–11]. This aspect is relevant also for masonry bridges, especially considering that most of them are older than 100 years [12,13]. Few studies investigated the effects of deterioration on the seismic response of masonry bridges [14,15].

This paper thus presented the derivation of a fragility model for masonry arch bridges affected by damage and deterioration. This study focused on single-span bridges due to their great significance in national inventories, compared to multi-span bridges. Fragility curves were evaluation for the macro-classes of segmental and semi-circular arches, and they represent the probability of exceeding either Damage (DLS) or Ultimate (ULS) Limit State. Typical defects of masonry bridges were included in the fragility assessment: (*i*) material loss at the intrados of the arch, (*ii*) material deterioration and (*iii*) the presence of longitudinal cracks in the arch barrel vault. Fragility curves were derived by processing data from parametric non-linear static analyses implemented on 2D finite element (FE) models developed in Diana [16]. Inter-structures variability was included by selecting a sample set of 32 bridges, whose geometric features were based on IrMB [2,4]. Multiple-stripe analysis (MSA) was implemented to include the record-to record variability, according to the procedure proposed by Shinozuka (2000) [17]. Further details on the implemented procedure can be found in Tecchio et al. (2022) [18]. Derived functions showed the impact of the investigated defects in increasing the seismic fragility of this type of bridges, in particular in case of material loss.

2 MODELLING AND ANALYSIS

Defects on masonry arch bridges have been generally classified acting on either foundation or superstructures [19]. Since this work focused on damage on the arch, the identification of typical damage and deterioration effects was dedicated to superstructures. Superstructures might be affected by the following damage and deterioration effects [20]: *i*) deterioration of material (e.g., decay and salt efflorescence); *ii*) loss of bricks and mortar joints; *iii*) deformation and detachment of the arch barrel; *iv*) deformation and detachment of spandrel walls; and *v*) cracks in piers and wing walls.

In this work, three main defects were selected to evaluate their effect on the seismic fragility of single-span bridges:

- localised material loss from the intrados of the arch barrel;
- generalised deterioration of material, with decrease of the mechanical properties;

- longitudinal cracking on the arch barrel at the interface with the voussoirs.

The effect of this damage and deterioration phenomena on the seismic fragility of masonry bridges was investigated through an analytical approach. A series of 2D finite element (FE) models were developed using TNO Diana [16], assuming plane strain state (Figure 1). The backfill was simulated in terms of mas only. As boundary conditions, fixed nodes were adopted at the springing of the arch.

The nonlinear behaviour of masonry was simulated through the *Total Strain Crack'* model, based on the smeared crack approach [21]. The compression response was assumed to be governed by a parabolic law, while the tensile behaviour was adopted as a linear softening. The values adopted as mechanical properties of masonry, according to various publications [22–24], are listed in Table 1.

Elastic Modulus	E	[MPa]	900.0
Density (masonry and backfill)	γ	[kN/m^3]	18.0
Poisson's ratio	ν	[-]	0.2
Compressive strength	f_c	[MPa]	5.0
Tensile strength	f_t	[MPa]	0.2
Compression fracture energy	G_c	[N/mm]	5.0
Tensile fracture energy	G_f	[N/mm]	0.0025

Table 1. Mechanical properties of masonry in FE modelling.

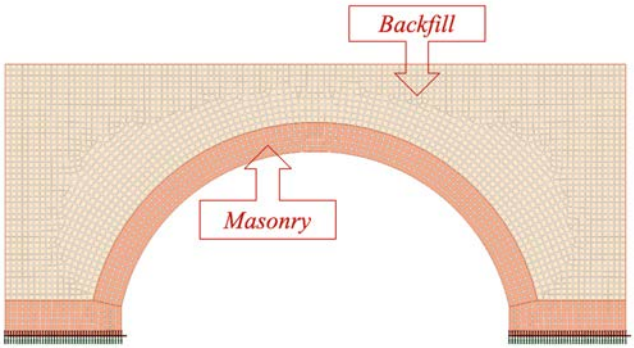

Figure 1. Adopted 2D FE modelling of masonry arch bridges.

The investigated effects of deterioration were modelled as follows. Material loss at the intrados was simulated by locally removing some finite elements, so as to model a reduced vault thickness in the damaged zone. Generalised material deterioration was modelled by worsening the mechanical properties of masonry. Since longitudinal cracking often leads to the voussoirs' detachment, it was associated to a reduction in the width of the barrel vault; thereby, in a 2D model, it was modelled by increasing the material density (γ), to simulate a redistribution of masses due to the reduced effective width of the vault. Two intensity levels were considered for each phenomenon, of slight and moderate deterioration, respectively.

The deterioration metric was assumed according to Kamiński and Bień (2013) [25]. The intensity of each deterioration effect was defined as the percentage ratio of the reduction (in geometric/material properties) to the undamaged quantity. For all investigated defects, two levels of intensity were adopted, equal to 5% and 20%.

Specifically, for material loss, the intensity (I_{ML}) is the ratio of the thickness of lost material (Δs) to the arch thickness (s) (Eq. 1). The damage was also described though two further

parameters expressing the extent (Δl) and location along the arch barrel (θ). The extent was deterministically assumed equal to 30 cm. Material loss was conservatively located in the most critical position, which was studied and presented in the next section. Material loss resulted more harmful when located at the third hinge of the potential longitudinal kinematic mechanism [4,26].

$$I_{ML} = \frac{\Delta s}{s} \cdot 100 \tag{1}$$

For material deterioration, the intensity (I_{MD}) consisted in the ratio of the reduction for damaged (ΔX_m) on undamaged values (X_m) of masonry properties (Eq. 2). A reducing factor (k_m) was assumed to calculate the reduced strength (f'_{cm}) and Young's modulus (E'_{cm}) of masonry (Eq. 3 and 4). The values of this factor corresponded to 0.95 and 0.8 for slight and moderate levels, respectively.

$$I_{MD} = \frac{\Delta X_m}{X_m} \cdot 100 \tag{2}$$

$$k_m = (1 - I_{MD}) \tag{3}$$

$$\begin{aligned} f'_{cm} &= k_m \cdot f_{cm} \\ E'_m &= k_m \cdot E_m \end{aligned} \tag{4}$$

For longitudinal cracking, the intensity (I_{CR}) depended on the reduction in width of the arch barrel (ΔW_B) and its original width (W_B) (Eq. 5). As aforementioned, this was simulated by increasing the mass acting on the barrel, to mimic the redistribution of vertical loads caused by the detachment of the arch outer bands. Thus, an increased material density (γ') was calculated through a magnifying factor (k_γ) (Eq. 6 and 7).

$$I_{CR} = \frac{\Delta W_B}{W_B} \cdot 100 \tag{5}$$

$$k_\gamma = (1 + I_{CR}) \tag{6}$$

$$\gamma' = k_\gamma \cdot \gamma \tag{7}$$

Figure 2 illustrates the investigated deterioration effects and their numerical simulation with the adopted metric.

3 FRAGILITY ASSESSMENT

3.1 Definition of sample datasets

This contribution attempts to quantifying the effect on the seismic fragility of damage and deterioration phenomena, focusing on single-span masonry arch bridges, as this macro-class represents the greatest portion in existing stocks available in the literature for the Italian framework [2,27]. In particular the inventory of masonry bridges of the Italian Railway network (IrMB) [2,4] provided the main geometric characteristics of single-span masonry bridges, illustrated in Figure 3.

Within the Italian Railway network, most single-span masonry bridges have an arch span up to 10 m long. Both segmental (46%) and semi-circular (42%) arches are well-represented. The former is characterised by a ratio of the arch rise (f) on span length (L) between 0.1 and 0.3, while the latter has values of f/L ranging from 0.4 to 0.5. The ratio of arch thickness (s) to span length showed values from 0.06 to about 0.2.

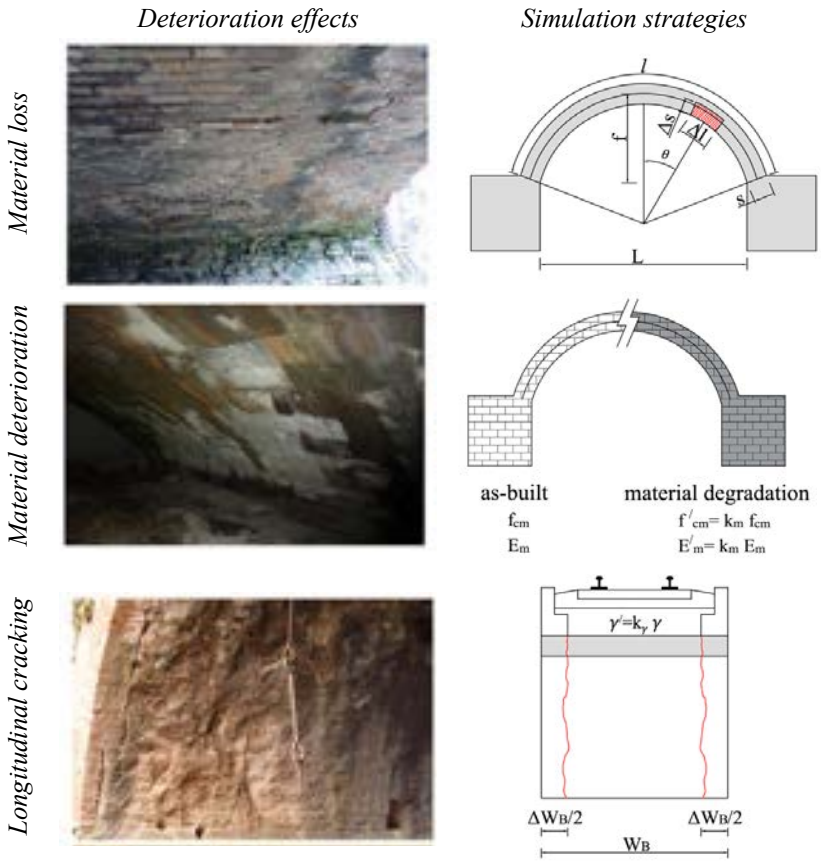

Figure 2. Deterioration effects and numerical simulation in TNO Diana [16].

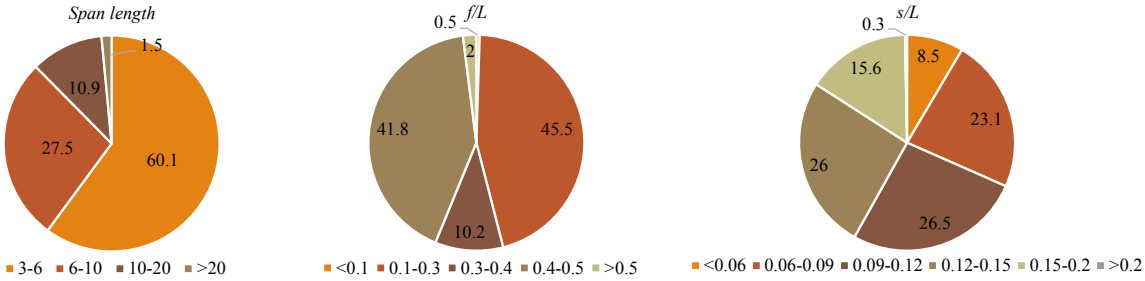

Figure 3. Distribution of geometric parameters of single-span bridges in IrMB [2,4].

Type	L [m]	f/L [-]	s/L [-]
Segmental	7 - 12	0.20 - 0.30	0.075 - 0.1
Semi-circular	7 - 12	0.40 - 0.50	0.075 - 0.1

Table 2. Ranges of geometric characteristics of sample bridges.

These distributions of geometric parameters were adopted to define two subsets of bridges, for segmental and semi-circular arches, respectively. Based on these subsets, 32 sample bridges were selected for each type. The ranges of values of geometric parameters for each subset are summarised in Table 2. Each sample bridge was analysed in the as-built configuration and then considering two levels of intensity of deterioration for each of the three investigated phenomena

(for a total of six damaged configurations). Thus, 224 models were implemented for as many nonlinear analyses.

3.2 Definition of performance levels and seismic demand

Adopted performance levels were selected to be compliant with regulations in force in Italy, and more generally in the European context [28–30]. Performance levels for Damage Limit State (DLS) and Ultimate Limit State (ULS) were identified on the bi-linearised curve derived from the generic capacity curve obtained from non-linear static analyses (by defining the secant period T_e and enforcing equality of subtended areas). Specifically, DLS coincided with the yield displacement (d_y), corresponding to the slope change in the bilinear curve, whereas ULS was adopted to be attained at the ultimate displacement (d_u), corresponding to 85% of the maximum resistance in the softening branch (Figure 4). For further details, please refer to Tecchio et al. (2022) [18].

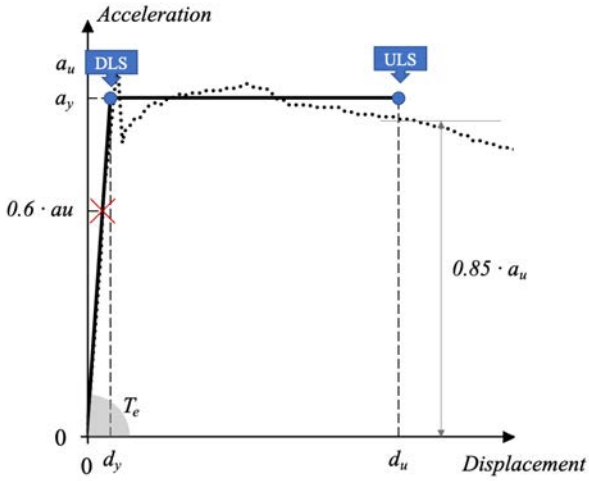

Figure 4. Identification of performance levels on bi-linearised capacity curve.

To include the uncertainty related to record-to-record variability in the fragility assessment, a Multiple-Stripe Analysis (MSA) was performed, also according to previous studies [4,17]. Four sets of ground motions were adopted. For each set, seven synthetic records were generated through SIMQKE software [31]. Synthetic accelerograms were assumed to be compatible with Type-1 spectra of Eurocode 8 [30], for soil A and values of peak ground acceleration (PGA) of 0.2, 0.4, 0.8 and 1.2 g.

To be compared with capacity curves from non-linear static analyses, selected ground motions were processed and represented in the period/frequency domain, as elastic acceleration spectra. Then, three reference spectra were computed for each PGA value: the average spectrum ($RS_m(T)$) and upper and lower bounds ($RS_m \pm \sigma_a(T)$) obtained by adding and subtracting the standard deviation of the spectral response (for each set of seven ground motions).

This for sets of reference spectra were then scaled to cover all values of PGA in the investigated interval (0.05-1.5 g). For some values of PGA double spectrum sets were considered, as also illustrated in Figure 5.

The obtained sets of scaled spectra, expressing the spectral pseudo-acceleration (Sa), were converted in displacement spectra according to equation 8.

$$S_d = S_a \left(\frac{T}{2\pi} \right)^2 \tag{8}$$

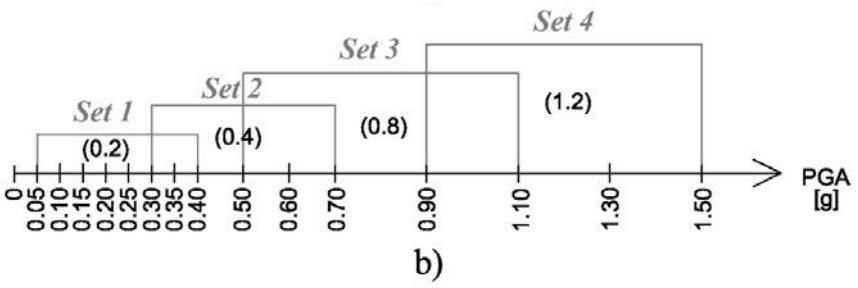

Figure 5. Intervals of PGA for scaling reference spectrum sets.

3.3 Derivation of fragility curves

Comparison of seismic demand and capacity was carried out in terms of displacement.

For the j^{th} bridge model, the displacement demand (Δ_{dem}) was evaluated based on displacement spectra and of the elastic period ($T_{e,j}$), according to the formulation of equation 9. Since three scaled spectra were considered, three displacement demand values were computed (Eq. 10).

$$\Delta_{dem} = S_d(T_e) \tag{9}$$

$$\Delta_{dem,j}{}^{k=1} = \overline{\Delta}_{dem,j} \;; \quad \Delta_{dem,j}{}^{k=2,3} = \overline{\Delta}_{dem,j} \pm \sigma_d \tag{10}$$

The displacement capacity of the j^{th} bridge ($\Delta_{cap,j}$) was calculated for each limit state as aforementioned (Figure 4).

Three measures of damage (DM_j^k) were calculated as illustrated in equation 11, as ratio of demand to capacity. Thus, a damage measure greater than unity denote the exceedance of the limit state.

$$DM_j{}^k = \Delta_{dem,j}{}^k / \Delta_{cap,j} \tag{11}$$

Through this procedure, clusters of *DM* values were obtained for each class of bridges (segmental and semi-circular), analysed configuration (both as-built and damaged, considering two levels of intensity), and for each limit state. These clusters were processed through least square linear regression, in the bi-logarithmic plane (*ln(PGA) vs ln(DM)*) (Eq. 12), to estimate the regression coefficients (*A* and *B*), expressing the probability of exceeding *DM* (Eq. 13 and 14)

$$\lambda = \ln\left(DM_m\right) = A + B\ln(PGA) \tag{12}$$

$$P_{f,PL}\ (\text{PGA}) = P\ [DM > dm_{PL} \mid \text{PGA}] = \int_{DM(PGA)>dm_{PL}} f_{DM}(dm \mid PGA)\ \mathrm{d}dm \tag{13}$$

$$f_{DM}(dm) = \frac{1}{\sqrt{2\pi}\varepsilon dm}\exp\left[-\frac{1}{2}\left(\frac{\ln dm - \lambda}{\varepsilon}\right)^2\right] \tag{14}$$

where λ is the logarithmic mean value of the damage and ε is the related logarithmic standard deviation.

The probability of exceeding *DM* was then used to fit the log-normal fragility curve expressing the attaining of a given limit state, defined by the median (μ) and the standard deviation (β), whose values are presented in Table 3.

		DLS		ULS	
		μ [g]	**β [-]**	**μ [g]**	**β [-]**
Segmental	As built	0.310	0.253	0.867	0.258
	Material loss				
	- Slight	0.282	0.290	0.781	0.296
	- Moderate	0.247	0.312	0.619	0.317
	Material degradation				
	- Slight	0.297	0.271	0.828	0.280
	- Moderate	0.284	0.245	0.786	0.249
	Longitudinal cracking				
	- Slight	0.292	0.265	0.824	0.273
	- Moderate	0.274	0.232	0.764	0.237
Semi-circular	As built	0.125	0.200	0.312	0.206
	Material loss				
	- Slight	0.115	0.198	0.286	0.201
	- Moderate	0.087	0.250	0.217	0.262
	Material degradation				
	- Slight	0.124	0.197	0.311	0.210
	- Moderate	0.120	0.187	0.300	0.193
	Longitudinal cracking				
	- Slight	0.121	0.189	0.303	0.194
	- Moderate	0.113	0.197	0.282	0.203

Table 3. Parameters of fragility curves for segmental and semi-circular arches in investigated configurations

4 COMPARISON OF RESULTS

The derived fragility curves for masonry arch bridges accounting for damage effects were compared with as-built fragilities in Figure 6. The values of median variation ($\Delta\mu$), between as-built and damaged responses, were calculated as showed in Eq. 15, and then summarised in Table 4 for both segmental and semi-circular arches.

$$\Delta\mu = \frac{\mu_{as-built} - \mu_{damaged}}{\mu_{as-built}} \tag{15}$$

The presence of defects was observed to affect the seismic vulnerability of this bridge type. However, the impact of various investigated defect varies significantly.

	Material loss		**Material deterioration**		**Longitudinal cracking**	
	DLS	**ULS**	**DLS**	**ULS**	**DLS**	**ULS**
			Segmental			
Slight	8.96 %	10.00 %	4.35 %	4.55 %	5.77 %	5.03 %
Moderate	20.22 %	28.66 %	8.42 %	9.36 %	11.51 %	11.90 %
			Semi-circular			
Slight	8.46 %	8.42 %	0.72 %	0.51 %	3.67 %	3.01 %
Moderate	30.57 %	30.53 %	4.31 %	3.84 %	9.98 %	9.83 %

Table 5. Percentage variation in median value (Δμ) between as-built and damaged conditions.

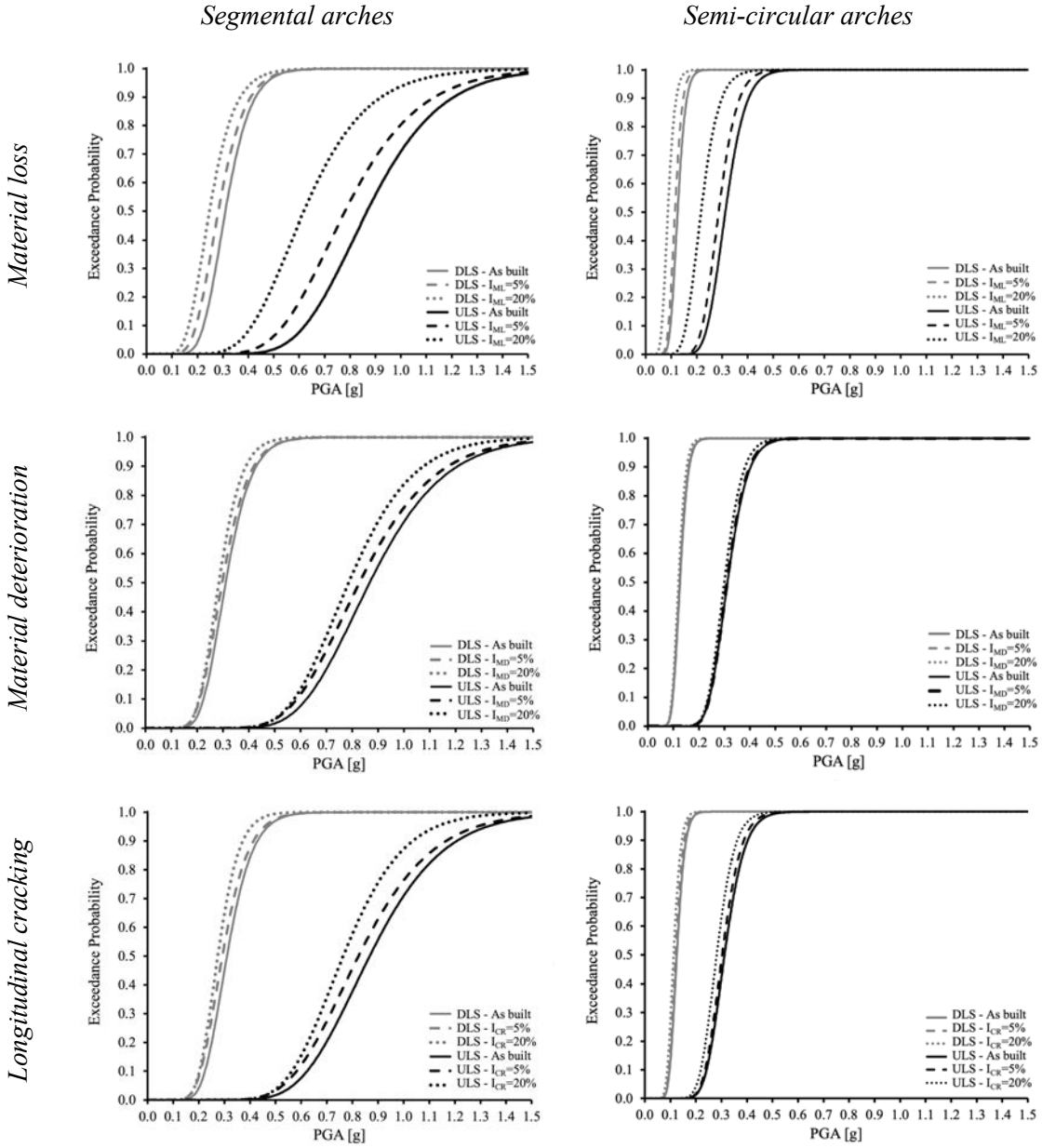

Figure 6. Comparison fragility curves of as-built and damaged configurations

Firstly, the as-built fragilities for the two classes of masonry arch bridges were comparable with comparable sets available in the literature and obtained through the well-established kinematic analysis [4].

In accordance with previous studies [4,32], semi-circular arches showed a generalised increased fragility compared to segmental bridges. Material loss at the intrados resulted the most impacting type of defects. When characterised by a slight intensity, its impact is rather similar for segmental and semi-circular arches, whereas material loss of moderate intensity (I_{ML} = 20%) appeared more severe for semi-circular bridges, with a reduction in the median value ($\Delta\mu$) of 31% for both DLS and ULS. This type of damage caused a reduction $\Delta\mu$ equal to 20% for DLS and to 29% for ULS, for segmental arches.

The other type of defects (material deterioration and longitudinal cracking) had a lower impact on the bridge seismic fragility. Both material deterioration and longitudinal cracking caused a lower reduction in the median value ($\Delta\mu$), thus having a lower influence on the

fragility, for semi-circular arches compared to segmental. This is in line with the fact that the seismic capacity of these bridges, especially semi-circular bridges, is strongly influenced by their geometric features, rather than by the mechanical properties of the masonry [33]. Nonetheless, the increase in fragility for material deterioration and longitudinal cracking was not negligible, especially in case of moderate intensity ($I_{MD} = I_{CR} = 20\%$). Based on the adopted metric, longitudinal cracking was more impacting than material deterioration.

5 CONCLUSIONS

- This paper aimed at providing a fragility model for masonry arch bridges, by also investigating the effect of typical defects of the arch barrel: (i) material loss at the vault intrados; (ii) widespread deterioration of masonry; (iii) longitudinal cracking of the arch barrel at the interface with the voussoirs. Fragility curves were derived for two macro-classes of single-span structures – i.e., segmental (f/L = 0.2 to 0.3) and semi-circular (f/L = 0.4 to 0.5) arches – both for the as-built and damaged configurations
- Parametric non-linear static analyses were implemented on 2D FE models developed in TNO Diana software. A sample dataset of 32 bridges was selected and then modelled in the as-built and damaged configurations, considering two intensity levels for each defect, for a total of 224 FE models and analyses.
- Material loss was modelled by locally reducing the arch thickness in the FE mesh, material deterioration was simulated by scaling the masonry properties, and longitudinal cracking by increasing vertical static loads.
- Comparisons between as built and damaged fragility curves showed the significant influence of material loss on the seismic vulnerability of these bridges. Indeed, for this type of damage, reductions in the median value of the log-normal functions ($\Delta\mu$) reached peaks of 31%, at both limit states, for semi-circular arch bridges. Other types of deterioration showed less impact.
- The different impact obtained for the investigated defects is very reasonable, considering that the seismic capacity of masonry arch bridges is mainly governed by geometric instability rather than by the material properties.
- Further studies need to be carried out to assess fragility for multi-span masonry arch bridges accounting for damage effects, also considering the defects of piers and foundations.

ACKNOWLEDGMENTS

Special thanks are due to the Italian Department of Civil Protection and ReLUIS, which funded this study in the framework of the ReLUIS-DPC Project 2022-2024 – Work Package 5 Task 4: Interventions on bridges.

REFERENCES

[1] D. Cocciaglia, L. Mosca, Capacità portante dei ponti ad arco ferroviari, La Tecnica Professionale. November 1 (1998).

[2] F. da Porto, G. Tecchio, P. Zampieri, C. Modena, A. Prota, Simplified seismic assessment of railway masonry arch bridges by limit analysis, Structure and Infrastructure Engineering. 12 (2015) 567–591. https://doi.org/10.1080/15732479.2015.1031141.

[3] D.M. Barbieri, Two methodological approaches to assess the seismic vulnerability of masonry bridges, Journal of Traffic and Transportation Engineering (English Edition). 6 (2019) 49–64. https://doi.org/10.1016/j.jtte.2018.09.003.

[4] G. Tecchio, M. Donà, F. da Porto, Seismic fragility curves of as-built single-span masonry arch bridges, Bulletin of Earthquake Engineering. 14 (2016) 3099–3124. https://doi.org/10.1007/s10518-016-9931-6.

[5] G. Tecchio, F. Lorenzoni, M. Caldon, M. Donà, F. da Porto, C. Modena, Monitoring of orthotropic steel decks for experimental evaluation of residual fatigue life, J Civ Struct Health Monit. 7 (2017) 517–539. https://doi.org/10.1007/s13349-017-0240-9.

[6] M. Domaneschi, A. De Gaetano, J.R. Casas, G.P. Cimellaro, Deteriorated seismic capacity assessment of reinforced concrete bridge piers in corrosive environment, Structural Concrete. 21 (2020) 1823–1838. https://doi.org/10.1002/suco.202000106.

[7] F. Cui, H. Li, X. Dong, B. Wang, J. Li, H. Xue, M. Qi, Improved time-dependent seismic fragility estimates for deteriorating RC bridge substructures exposed to chloride attack, Advances in Structural Engineering. 24 (2021) 437–452. https://doi.org/10.1177/1369433220956812.

[8] P. Gardoni, D. Rosowsky, Seismic fragility increment functions for deteriorating reinforced concrete bridges, Structure and Infrastructure Engineering. 7 (2011) 869–879. https://doi.org/10.1080/15732470903071338.

[9] J. Ghosh, J.E. Padgett, Aging considerations in the development of time-dependent seismic fragility curves, Journal of Structural Engineering. 136 (2010) 1497–1511. https://doi.org/10.1061/(ASCE)ST.1943-541X.0000260.

[10] R. Kliukas, O. Lukoševičiene, A. Juozapaitis, A time-dependent reliability prediction of deteriorating spun concrete bridge piers, European Journal of Environmental and Civil Engineering. 19 (2015) 1202–1215. https://doi.org/10.1080/19648189.2015.1008650.

[11] J. Zhong, P. Gardoni, D. Rosowsky, Seismic fragility estimates for corroding reinforced concrete bridges, Structure and Infrastructure Engineering. 8 (2012) 55–69. https://doi.org/10.1080/15732470903241881.

[12] C. Melbourne, J. Wang, A.K. Tomor, A new masonry arch bridge assessment strategy (SMART), Proceedings of the Institution of Civil Engineers: Bridge Engineering. 160 (2007) 81–87. https://doi.org/10.1680/bren.2007.160.2.81.

[13] SB-ICA, Guideline for Inspection and Condition Assessment of Existing European Railway Bridges - Including advices on the use of non-destructive testing, Sustainable Bridges. (2007) 1–259.

[14] A. Benedetti, J. Nichols, A. Tomor, Influence of environmental degradation on dynamic properties of masonry bridges, Brick and Block Masonry: Trends, Innovations and Challenges - Proceedings of the 16th International Brick and Block Masonry Conference, IBMAC 2016. (2016) 1029–1036. https://doi.org/10.1201/b21889-129.

[15] P. Zampieri, M.A. Zanini, F. Faleschini, Influence of damage on the seismic failure analysis of masonry arches, Constr Build Mater. 119 (2016) 343–355. https://doi.org/10.1016/j.conbuildmat.2016.05.024.

[16] TNO Diana v.9.6 User's Manual, (2014). https://dianafea.com/manuals/d96/Diana.html.

[17] M. Shinozuka, M.Q. Feng, H.-K. Kim, S. Kim, Nonlinear Static Procedure for Fragility Curve Development, J Eng Mech. 126 (2000) 1287–1295. https://doi.org/10.1061/(asce)0733-9399(2000)126:12(1287).

[18] G. Tecchio, M. Donà, E. Saler, F. da Porto, Fragility of single-span masonry arch bridges accounting for deterioration and damage effects, European Journal of Environmental and Civil Engineering. (2022). https://doi.org/10.1080/19648189.2022.2108504.

[19] R. Ozaeta García-Catalán, J.A. Martín-Caro, Catalogue of Damages in masonry arch bridges, International Union of Railways (UIC), Paris, France, 2020. https://www.shop-etf.com/en/catalogue-of-damages-in-masonry-arch-bridges.html?mc_cid=85ec56f8ba&mc_eid=2b4aa962aa.

[20] C. Modena, G. Tecchio, C. Pellegrino, F. da Porto, M. Donà, P. Zampieri, M.A. Zanini, Reinforced concrete and masonry arch bridges in seismic areas: typical deficiencies and retrofitting strategies, Structure and Infrastructure Engineering. 11 (2015) 415–442. https://doi.org/10.1080/15732479.2014.951859.

[21] J.G. Rots, Smeared and discrete representations of localized fracture, Int J Fract. 51 (1991) 45–59. https://doi.org/10.1007/BF00020852.

[22] D. V. Oliveira, P.B. Lourenço, C. Lemos, Geometric issues and ultimate load capacity of masonry arch bridges from the northwest Iberian Peninsula, Eng Struct. 32 (2010) 3955–3965. https://doi.org/10.1016/j.engstruct.2010.09.006.

[23] L. Pelà, A. Aprile, A. Benedetti, Seismic assessment of masonry arch bridges, Eng Struct. 31 (2009) 1777–1788. https://doi.org/10.1016/j.engstruct.2009.02.012.

[24] A. Brencich, U. De Francesco, Assessment of Multispan Masonry Arch Bridges. II: Examples and Applications, Journal of Bridge Engineering. 9 (2004) 591–598. https://doi.org/10.1061/(asce)1084-0702(2004)9:6(591).

[25] T. Kamiński, J. Bień, Application of kinematic method and FEM in analysis of ultimate load bearing capacity of damaged masonry arch bridges, Procedia Eng. 57 (2013) 524–532. https://doi.org/10.1016/j.proeng.2013.04.067.

[26] F. Fabbrocino, G. Ramaglia, G.P. Lignola, A. Prota, Ductility-based incremental analysis of curved masonry structures, Eng Fail Anal. 97 (2019) 653–675. https://doi.org/10.1016/j.engfailanal.2019.01.027.

[27] E. Saler, M. Donà, V. Pernechele, G. Tecchio, F. da Porto, Characterisation of an urban bridge portfolio and multi-risk prioritisation accounting for deterioration and seismic vulnerability, International Journal of Disaster Risk Reduction. 87 (2023). https://doi.org/10.1016/j.ijdrr.2023.103596.

[28] NTC2018 - D.M. 17/01/2018, Aggiornamento delle “Norme tecniche per le costruzioni” (in Italian), Official Gazzette of Italian Republic N°42 of 20th February 2018. (2018).

[29] Circ 21/01/2019 N.7, Istruzioni per l’applicazione dell’«Aggiornamento delle “Norme tecniche per le costruzioni”» di cui al decreto ministeriale 17 gennaio 2018. (in Italian), Official Gazzette of Italian Republic N°35 of 11th February 2019. (2019) 337.

[30] CEN, (European Committee for Standardization) EN1998 Eurocode 8-1: Design of structures for earthquake resistance. Part 1: General rules, seismic actions and rules for buildings, 144 (2004) 55–60. https://doi.org/10.1680/cien.144.6.55.40618.

[31] D.A. Gasparini, E.H. Vanmarcke, Simulated earthquake motions compatible with prescribed response spectra, MIT Department of Civil Engineering Research Report, 1976.

[32] P. Clemente, A. Raithel, The mechanism model in the seismic check of stone arches, in: A. Sinopoli (Ed.), Arch Bridges: History, Analysis, Assessment, Maintenance and Repair., 1st Editio, CRC Press, Balkema, Rotterdam, 1998: pp. 123–129.

[33] L. De Lorenzis, M. DeJong, J. Ochsendorf, Failure of masonry arches under impulse base motion, Earthq Eng Struct Dyn. 36 (2007) 2119–2136. https://doi.org/10.1002/eqe.719.